IOPscience iopscience.iop.org

Home Search Collections Journals About Contact us My IOPscience

Relation of conduction changes and magnetic properties in $Nd_{1-x}Pb_xMnO_3$ ($0.10 \leq x \leq 0.25$)

This article has been downloaded from IOPscience. Please scroll down to see the full text article.

2004 J. Phys.: Condens. Matter 16 1061

(http://iopscience.iop.org/0953-8984/16/7/006)

View the table of contents for this issue, or go to the journal homepage for more

Download details:
IP Address: 129.252.86.83
The article was downloaded on 27/05/2010 at 12:44

Please note that terms and conditions apply.

INSTITUTE OF PHYSICS PUBLISHING JOURNAL OF PHYSICS: CONDENSED MATTER

J. Phys.: Condens. Matter **16** (2004) 1061–1073 PII: S0953-8984(04)72497-2

Relation of conduction changes and magnetic properties in $Nd_{1-x}Pb_xMnO_3$ ($0.10 \leqslant x \leqslant 0.25$)

S Komine[1] **and E Iguchi**[2]

Division of Materials Science and Engineering, Graduate School of Engineering, Yokohama National University, Tokiwadai, Hodogaya-Ku, Yokohama 240-8501, Japan

E-mail: iguchi@post.me.ynu.ac.jp

Received 26 November 2003
Published 6 February 2004
Online at stacks.iop.org/JPhysCM/16/1061 (DOI: 10.1088/0953-8984/16/7/006)

Abstract

Measurements of bulk conductivity and dielectric relaxation processes by ac methods including complex-plane impedance analyses have been carried out on insulating $Nd_{1-x}Pb_xMnO_3$ ($0.10 \leqslant x \leqslant 0.25$), together with measurements of four-probe dc conductivity and magnetic susceptibility, so as to investigate the correlation between bulk conduction and short-range ferromagnetism due to double-exchange (DE) interactions working even above ferromagnetic ordering temperature (T_c). In bulk conduction, there are three temperature regimes where different processes dominate the electronic conduction: (i) the paramagnetic regime above the temperature at the onset of deviation of inverse magnetic susceptibility from the Curie–Weiss law, (ii) the intermediate regime and (iii) the temperature region below T_c. Though the polaronic conduction occurs in both high-temperature and intermediate regions, the hopping energy and the energy required to create a free hopping polaron differ considerably in these regimes. An anomaly emerges in both bulk conduction and dielectric relaxation processes around T_c at $x = 0.20$ and this anomaly becomes more clear at $x = 0.25$. By taking account of electron–phonon interactions, these results are discussed mainly in terms of the DE mechanism that brings about short-range ferromagnetism.

1. Introduction

Hole-doped perovskite manganites have attracted much attention in the sense that they exhibit unusual magnetic and transport properties [1]. In particular, the colossal magnetoresistance effect and the metal–insulator (MI) transition with the ferromagnetic to paramagnetic transition

[1] Present address: Seimi Chemical Co. Ltd, Chigasaki 3-2-10, Chigasaki 253-8585, Japan.
[2] Author to whom any correspondence should be addressed.

 © 2004 IOP Publishing Ltd Printed in the UK

are not only very interesting from the scientific point of view but also significantly important industrially [2–4]. Besides magnetic and transport properties of hole-doped perovskite manganites, structural investigations using the small-angle neutron scattering method and so on have been carried out very carefully because they are related each other very closely [5].

Two end members of the perovskite manganites which are of great interest at the moment are $LaMnO_3$ and $NdMnO_3$. Because the ionic radius of La^{3+} is larger than Nd^{3+}, $LaMnO_3$ is less distorted than $NdMnO_3$. When divalent alkaline elements are substituted for La^{3+} or Nd^{3+} in these oxides, the differences in ionic sizes ease lattice strain or increase distortion. In less strained manganites like $La_{1-x}A_xMnO_3$, Mn-e_g electrons are more itinerant because of the short Mn–O bond length and the small deviation of Mn–O–Mn bond angle from 180° and, consequently, the conductivity is high, where A is a divalent alkaline element [6, 7]. Furthermore, these manganites exhibit metallic conduction due to double-exchange (DE) interactions in ferromagnetic regimes [2, 3, 8–10]. In more distorted manganites such as $Nd_{1-x}A_xMnO_3$, however, the long Mn–O bond length and the rather large deviation of Mn–O–Mn bond angle from 180° attenuate the DE interactions even at low temperature. In such manganites, electron–phonon (EP) interactions are active and then the insulating behaviours with weak ferromagnetism are predominant [11]. As a feature of manganites, Jahn–Teller (JT) distortion must make some significant contribution to EP interactions [12–14]. The subtle competition between DE and EP interactions must be one of the most important parameters in creating the MI transition, where both the interactions are governed by lattice parameters such as Mn–O bond length and Mn–O–Mn bond angle.

Below the ferromagnetic ordering temperature (Curie temperature; T_c), many manganites involve charge orderings that bring about antiferromagnetic or ferromagnetic insulator phases [15–20]. On the other hand, short-range ferromagnetic interaction due to the DE mechanism works even at $T > T_c$ and causes macroscopic deviation from the Curie–Weiss law [5]. Furthermore, short-range ferromagnetism gives rise to the anomalous expansible volume lattice distortion which has relevance to localized carriers at $T > T_c$ [5, 21–23]. A negative magnetoresistance and a shift of the MI transition point to a higher temperature in most manganites under the action of an applied magnetic field are also ascribed to short-range ferromagnetism [5].

Because of these complicated phenomena, transport properties in many manganites are very difficult to clarify and still in dispute. At higher temperature, manganites contain paramagnetic regimes subject to Curie–Weiss law. Since short-range ferromagnetism must be annihilated in the paramagnetic regime, some change in the conduction process is expected at the transition from the paramagnetic regime to the region including the deviation from the Curie–Weiss law because the short-range ferromagnetism alters the natures of carriers. There is, however, no literature that observes such a change of the conduction process. This change must be then very difficult to recognize in measurements of the dc conductivity that includes the boundary effect. The bulk conductivity obtained by the complex-plane impedance analysis could detect this change of the conduction process [24–31]. From this point of view, therefore, it is of great interest to elucidate the correlation between the conduction and the short-range ferromagnetism working even at $T > T_c$ by measuring the bulk conductivity.

$Nd_{1-x}Ca_xMnO_3$ exhibits insulating conduction, but $Nd_{1-x}Sr_xMnO_3$ involves metallic conduction in the ferromagnetic regime at $T < T_c$ even if x is very small, because Sr^{2+} has an ionic radius bigger than Ca^{2+} [18, 32]. This indicates a strong relationship between the electronic conduction and the lattice distortion. Since DE and EP interactions depend upon the lattice distortion, the competition between these interactions is one of the parameters that dominate the conduction type. Variation of the lattice distortion by changing the amount of the substitute A could clarify the relationship of DE and EP interactions in the electronic

conduction. Despite the different conduction types in $Nd_{1-x}Ca_xMnO_3$ and $Nd_{1-x}Sr_xMnO_3$, the majority carriers in electronic transport and magnetic properties are Mn-e_g electrons.

Referring to our previous reports indicating that the ac measurement including the complex-plane impedance analysis provides significant knowledge of transport properties in insulating oxides [28, 33–35], the present study treats $Nd_{1-x}Pb_xMnO_3$ ($0.10 \leqslant x \leqslant 0.25$) because this oxide system in this composition range exhibits insulating behaviours with rather high resistivity. Moreover, variation of the lattice distortion is possible by changing the amount of Pb. When x is greater than 0.30, the high conductivity interferes with ac measurements because of the large electronic polarization effect.

2. Experimental details

Polycrystalline $Nd_{1-x}Pb_xMnO_3$ specimens ($x = 0.10$, 0.15, 0.20 and 0.25) were prepared by the conventional solid-state reaction technique using Nd_2O_3, PbO_2 and Mn_2O_3 powders (4 N). The mixtures were calcined in flowing pure oxygen at 900 °C for one day. After grinding the powders, this heating treatment was repeated. The powders were then pressed into pellets, and finally sintered in flowing pure oxygen at 1150 °C for one day. The powder diffraction using a Cu Kα x-ray indicates a single phase for every specimen. The lattice constants at room temperature are $a = 5.443$ Å, $b = 5.522$ Å, $c = 7.689$ Å at $x = 0.10$, $a = 5.448$ Å, $b = 5.501$ Å, $c = 7.706$ Å at $x = 0.15$, $a = 5.452$ Å, $b = 5.496$ Å, $c = 7.691$ Å at $x = 0.20$ and $a = 5.468$ Å, $b = 5.511$ Å, $c = 7.693$ Å at $x = 0.25$. Though $NdMnO_3$, the end member in the present system, is orthorhombic, the crystal structure becomes close to rhombohedral with increasing x [36].

Ac measurements (capacitances and impedances) have been carried out in the same way as the previous reports [28, 35] using HP 4284A LCR meters with a frequency range of 50 Hz to 1 MHz. Flat surfaces of the specimens were coated with an In–Ga alloy in a 7:3 ratio by a rubbing technique for the electrodes. Evaporated gold was also used for the electrode, but no significant difference was found in experimental results. A Maxwell–Wagner type polarization due to heterogeneity in a specimen is excluded because there are no significant differences in frequency dependence of dielectric constant at room temperature even if the thickness of the specimen is reduced to half. The details of the dc measurement by the four-probe method are described elsewhere [28, 29]. A copper–constantan thermocouple precalibrated at 4.2, 77 and 273 K was used for the temperature measurements.

The molar magnetic susceptibilities, χ, were measured using a Quantum Design superconducting interference device magnetometer (SQUID) with an applied field of $B = 0.01$ T in the temperature range of 10–300 K.

3. Experimental results

Figure 1 shows the temperature dependences of χ^{-1} for the specimens with $x = 0.10$ and 0.25. Others ($x = 0.15$ and 0.20) exhibit similar behaviours. The susceptibility χ in every specimen is plotted against T in the inset, which shows an increase in χ with increasing x. The relation of χ^{-1} and T contains a linear portion at $T > 222$ K for $x = 0.10$, $T > 226$ K for $x = 0.15$, $T > 207$ K for $x = 0.20$ and $T > 210$ K for $x = 0.25$. Then the Curie–Weiss law holds in every specimen. The temperature which marks the onset of the deviation of χ^{-1} from the Curie–Weiss law is abbreviated as T_p. Such a deviation is often observed in manganites which include short-range ferromagnetism owing to the DE interactions above the ferromagnetic ordering temperature T_c [5, 21–23]. Though $NdMnO_3$ exhibits antiferromagnetism at lower

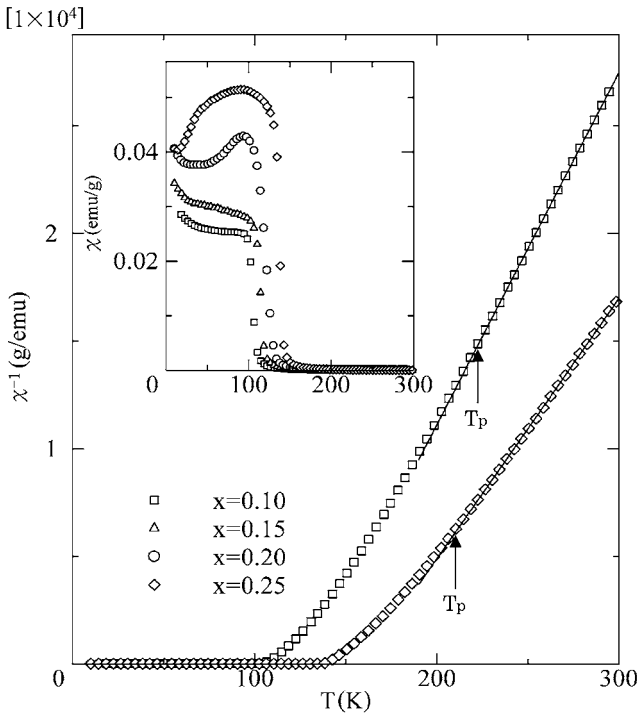

Figure 1. χ^{-1} versus T at $x = 0.10$ and 0.25 with arrows of T_p which mark onsets of deviation from the Curie–Weiss law. Other specimens with $x = 0.15$ and 0.20 exhibit similar behaviours. The inset shows the relation of χ versus T for every specimen.

temperature, $Nd_{1-x}Pb_xMnO_3$ contains the ferromagnetic regime as shown in figure 1. Arrott plots yield $T_c = 107$, 117, 124 and 139 K for $x = 0.10$, 0.15, 0.20 and 0.25. As x increases, T_c rises.

The conductivity measurements of single crystals provide very significant knowledge of electronic transport, but the present study uses sintered polycrystalline specimens. Even in such a polycrystalline specimen, however, the complex-plane impedance analysis can distinguish the bulk conduction from others [24–30]. Following the detailed account of the theoretical treatment of the impedance analysis [24–27], the resistance values in bulks and grain boundaries are estimated.

Figure 2 depicts complex-plane impedance plots at 110, 150 and 190 K for the specimen with $x = 0.15$. These plots contain a two-semicircular-arc structure, i.e., the highest-frequency arc due to the bulk conduction and the intermediate-frequency arc resulting from the conduction across boundaries.

Employing three sorts of conductivity, i.e., the bulk conductivity, the total conductivity transformed from the sum of the resistances in bulks and boundaries, and the four-probe dc conductivity [28–31], figure 3 demonstrates three Arrhenius relations of $\sigma \cdot T$ and $1/T$ for the specimen with $x = 0.10$. These plots are based upon the theoretical formula for the conductivity due to a hopping process of adiabatic small polarons, which will be described in the discussion section. Though the straight lines are also obtained if these conductivities are plotted in the Arrhenius relation of σ and $1/T$, the activation energies differ from the real values required for the hopping processes. Though the total conductivities are experimentally

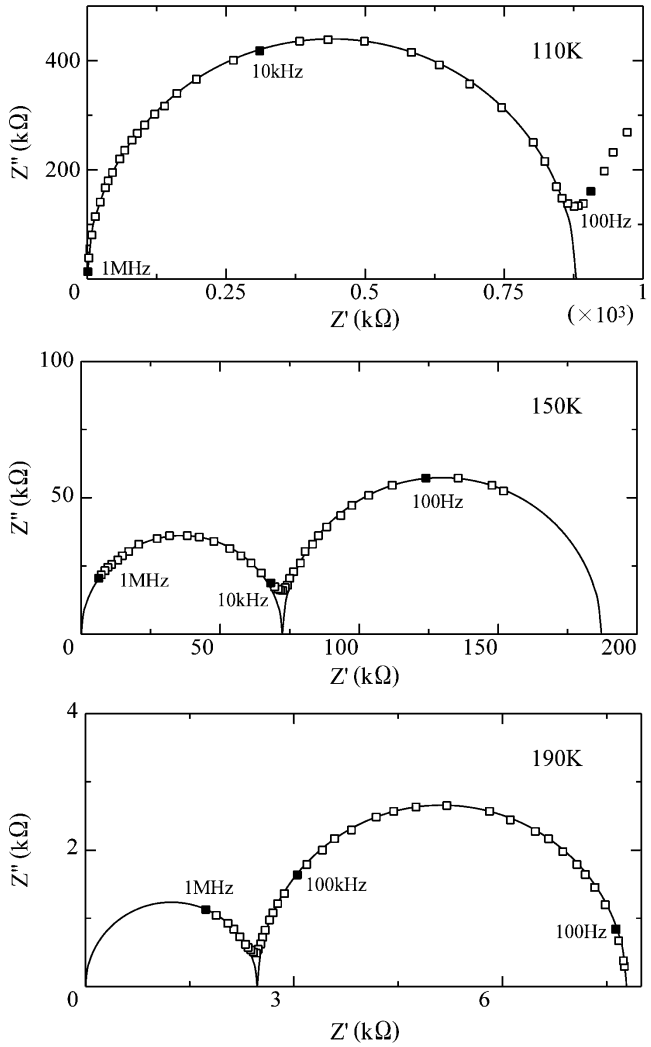

Figure 2. Complex-plane impedance analyses for the specimen with $x = 0.15$ at 110, 150 and 190 K.

available only at $T > 140$ K, they are in very good agreement with dc conductivities. This fact indicates the legitimacy of the impedance analysis and then the bulk conductivities obtained by this analysis are very reliable. The bulk conduction consists of three processes, i.e., the high-temperature process above ∼225 K, the intermediate one between ∼225 K and T_c and the low-temperature one below T_c. The transition around 225 K is enlarged in the inset of figure 3. The four-probe dc conductivity measurement never recognizes this transition. Since the transition temperature, ∼225 K, is nearly equal to $T_p = 222$ K, the onset of the deviation from the Curie–Weiss law and the change of the conduction process around 225 K must have the same origin.

The impedance analysis is possible to carry out in the range 82–260 K for the specimen with $x = 0.10$. There is then a limited frequency region in which bulk conductivities are measurable. Other specimens exhibit similar behaviours. Employing the bulk conductivities,

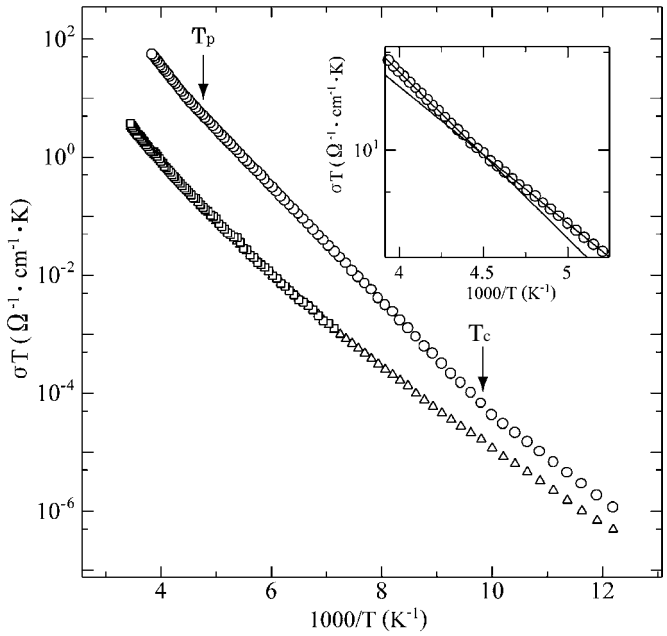

Figure 3. Three Arrhenius relations of σT versus $1/T$ at $x = 0.10$: the bulk conductivity (○), the conductivity estimated from the highest resistance of the intermediate semicircular arc (□) and the four-probe dc conductivity (△). The inset enlarges the Arrhenius relation of the bulk conductivity around 225 K. T_p and T_c are indicated on the bulk conductivity.

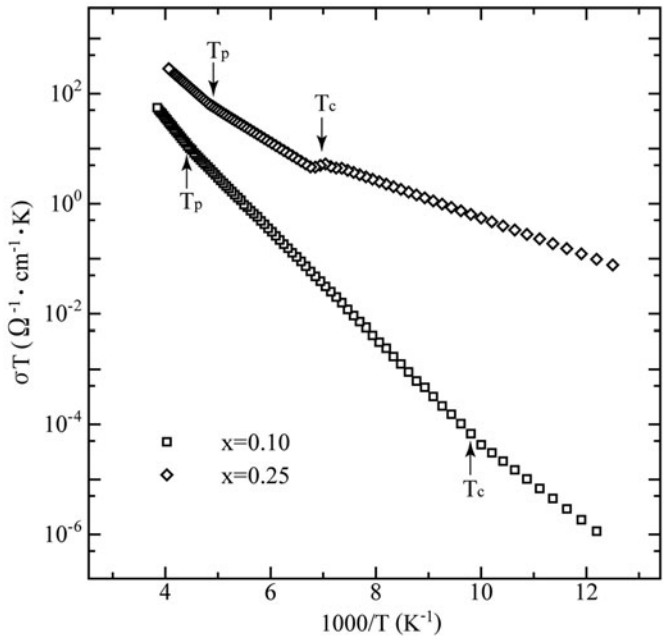

Figure 4. Arrhenius plots of σT versus $1/T$ for $x = 0.10$ and 0.25 with arrows marking T_p and T_c, where σ is the bulk conductivity.

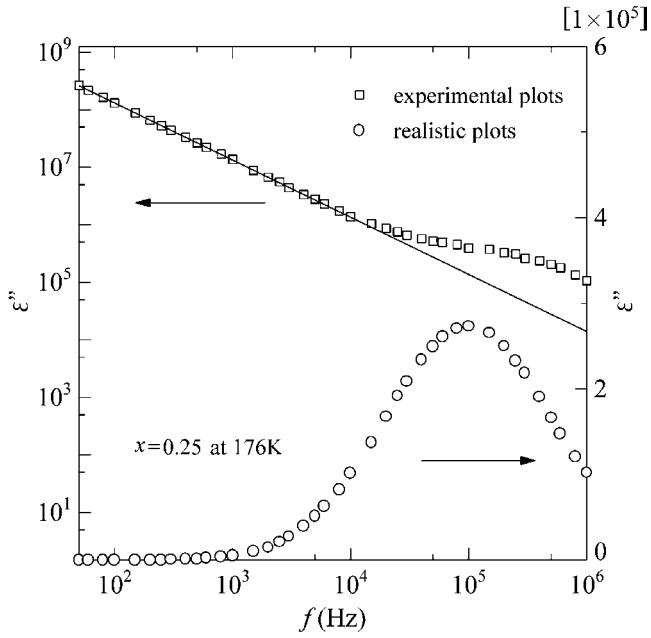

Figure 5. Frequency dependence of the dielectric loss factor ε'' with the realistic dielectric loss factor for the specimen with $x = 0.25$ at 176 K, where the realistic dielectric loss factor is the magnitude after the low-frequency contribution has been subtracted. The straight line represents the low-frequency contribution.

figure 4 demonstrates the Arrhenius plots of $\sigma \cdot T$ and $1/T$ for the specimens with $x = 0.10$ and 0.25.

A relaxation process shows up in dielectric properties such as loss factor for every specimen. Figure 5 displays the frequency dependence of dielectric loss factor ε'' at 176 K for the specimen with $x = 0.25$ with the realistic dielectric loss factor obtained by subtracting low-frequency contributions in a similar way to the previous treatment [33, 34, 37]. The realistic dielectric loss factor is also plotted as a function of applied frequency f as a parametric function of temperature at 2 K increments for the specimen with $x = 0.10$ in figure 6. The loss factor at the applied frequency of 50 Hz to 1 MHz is measurable in the temperature region of 150–290 K at $x = 0.10$. At each temperature, the dielectric loss factor has the maximum $\varepsilon''_{\max}$ at the resonance frequency $f_{\varepsilon''_{\max}}$. In the region of 170–290 K, $f_{\varepsilon''_{\max}}$ and $\varepsilon''_{\max}$ increase regularly with increasing T, although the slope of $(\mathrm{d}\varepsilon''_{\max}/\mathrm{d}f)$ changes around $T_p \cong 226$ K. Below 170 K, $f_{\varepsilon''_{\max}}$ is less than 10^3 Hz and there is some disarray in the relative positions of the peak heights $\varepsilon''_{\max}$. It is rather difficult to subtract low-frequency contributions properly at $f_{\varepsilon''_{\max}} < 10^3$ Hz, but $f_{\varepsilon''_{\max}}$ is definitely determinable even below 170 K. Other specimens exhibit dielectric behaviours similar to that of $x = 0.10$, but the temperature region in which the loss factor is measurable changes from specimen to specimen.

4. Discussion

4.1. Bulk conduction in high-temperature region at $T > T_p$

The most significant aspect of the bulk conduction in figure 4 is that there are three temperature regimes where different processes dominate the conduction as described in the previous

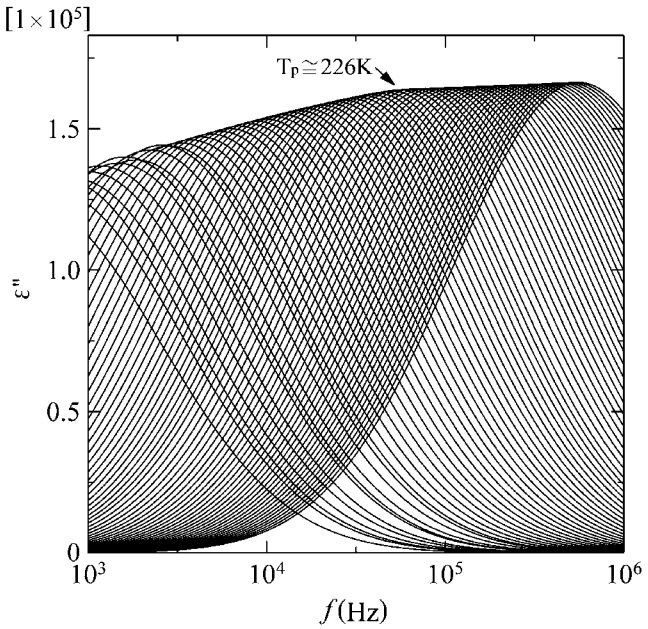

Figure 6. Frequency dependences of realistic dielectric loss factor ε'' as a parametric function of temperature at 2 K increments for the specimen with $x = 0.10$.

section. The bulk conductivity increases as hole doping proceeds with increasing x. In many insulating oxides, a hopping process of small polarons dominates the electronic conduction in paramagnetic regimes [5, 28, 29, 33–35, 38–43]. The conductivity due to the hopping process of adiabatic small polarons has the form of $\sigma = (A_0/T)\exp\{-(W_H + W_O/2)/k_B T\}$, where A_0 is a constant, k_B is the Boltzmann constant, W_H is the hopping energy of a polaron and W_O is the energy required to create a free hopping polaron, i.e., the potential difference between a polaron bound to a trap and a free hopping polaron [44–46]. Small polarons of holes created by Pb substitution for Nd are bound to traps at low temperature and they are thermally activated to mobile hopping polarons. Then W_O is the trapping energy. The concentration of the free hopping polarons in thermal equilibrium is proportional to $\exp(-W_O/2k_B T)$. From this point of view, figure 4 plots the Arrhenius relation of $\sigma \cdot T$ and $1/T$. In the paramagnetic regime at $T > T_p$, each specimen contains a linear portion. The least squares methods yield $(W_H + W_O/2) = 0.24$, 0.20, 0.18 and 0.17 eV for $x = 0.10$, 0.15, 0.20 and 0.25.

The transport result in figure 4 then certainly favours the polaronic scenario in the bulk conduction at $T > T_p$ and this scenario is also evident from ac experiments. The dielectric behaviours in the present study are approximately described by Debye's theory [47]. The dielectric resonance condition due to polaron hopping has the form of $f_{\varepsilon''_{max}} \propto \exp(-W_H/k_B T)$ at a temperature T [31, 41]. Using the experimental values for $f_{\varepsilon''_{max}}$ determined in the relation of ε'' and f, the Arrhenius relations of $f_{\varepsilon''_{max}}$ and $1/T$ are illustrated in figure 7, where only the plots above ∼150 K are available at $x = 0.10$ and 0.15. In every specimen, an appreciable transition is found at T_p and there is a linear portion at $T > T_p$. The least-squares methods yield $W_H = 0.21$, 0.17, 0.16 and 0.14 eV for $x = 0.10$, 0.15, 0.20 and 0.25. The hopping energy decreases with increasing x because the lattice becomes less distorted.

The increase in the maximum of the dielectric loss factor ε''_{max} with increasing T in figure 6 suggests thermal excitation in the intensity of the dielectric relaxation. The maximum

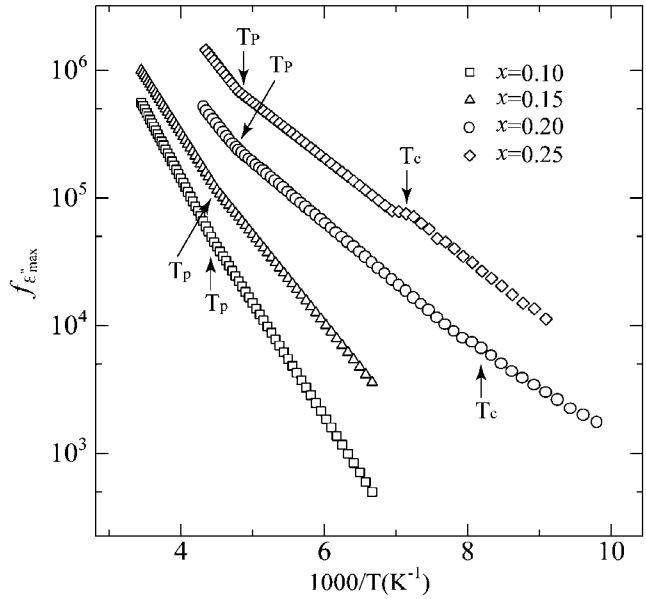

Figure 7. Arrhenius relation between $f_{\varepsilon''_{max}}$ and $1/T$ for every specimen with arrows indicating T_p and T_c.

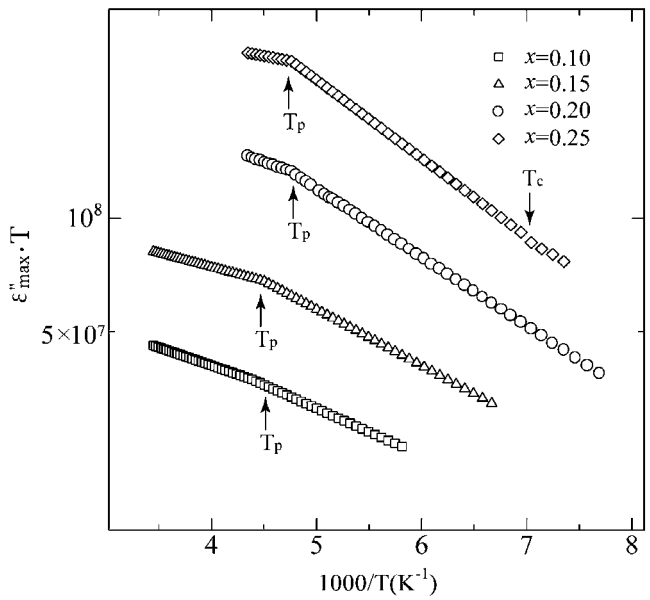

Figure 8. Arrhenius relation between $\varepsilon''_{max} \cdot T$ and $1/T$ for every specimen with arrows indicating T_p and T_c.

of the dielectric loss factor ε''_{max} is theoretically proportional to the amount of the hopping carriers in the polaronic conduction [31, 45]. At a temperature T, one has the relation $\varepsilon''_{max} \propto \exp(-W_O/2k_BT)/T$. Figure 8 depicts the Arrhenius plots of $\varepsilon''_{max} \cdot T$ and $1/T$. In every specimen, the marked transition is found at T_p and there is a linear portion above

T_p and also below T_p. The activation energies W_O at $T > T_p$ are 0.036, 0.036, 0.034 and 0.028 eV for $x = 0.10$, 0.15, 0.20 and 0.25. Then the sum of W_H and $W_O/2$, both obtained in ac measurements, is nearly equal to the activation energy required for the bulk conduction above T_p. Consequently, a hopping process of small polarons governs the conduction in $Nd_{1-x}Pb_xMnO_3$ ($x \leqslant 0.25$) at $T > T_p$ as well as many insulating paramagnetic oxides. Referring to the intrinsic nature of Mn^{3+} [5, 6, 19], one expects some important contribution of the JT effect in polaron formation and the polaron in the present oxide system must involve a rather strong JT component. However, the means employed here cannot distinguish the JT component from others.

4.2. Bulk conduction in intermediate region between T_p and T_c

Every specimen undergoes the transition from the high-temperature region to the intermediate process at T_p. Since this transition seems impossible to observe in the four-probe dc measurements, the impedance analysis and ac measurements are indispensable in the present oxide system. In the intermediate region between T_p and T_c, the bulk conductivity and the dielectric loss factor are also subject to the theoretical behaviours based upon a hopping process of adiabatic small polarons. The least-squares methods in this region of figures 4, 7 and 8 yield $(W_H + W_O/2) = 0.19$, 0.16, 0.13 and 0.12 eV, $W_H = 0.17$, 0.13, 0.098 and 0.084 eV, and $W_O = 0.050$, 0.059, 0.074 and 0.080 eV for $x = 0.10$, 0.15, 0.20 and 0.25. Then the sum of W_H and $W_O/2$ is nearly equal to the activation energy in the bulk conduction $(W_H + W_O/2)$ for every specimen. In comparison with the high-temperature region at $T > T_p$, however, the hopping energy W_H is low and decreases more rapidly with increasing x.

Such a low hopping energy is probably ascribable to the DE interactions due to the magnetic coupling between Mn^{3+} and Mn^{4+} through O^{2-} resulting from the motion of an electron between the two partially filled d shells with strong on-site Hund coupling [8]. Hole doping increases the amount of Mn^{3+} which plays an essential role in the DE mechanism. Magnetic moments on Mn sites under the action of the DE interactions tend to line up parallel to each other, consequently resulting in short-range ferromagnetism and an increase in the electron transfer integral t, which somewhat broadens the band width. Short-range ferromagnetism is involved even above T_c in many manganites such as $La_{0.67}Ca_{0.33}Mn_{0.9}Fe_{0.1}O_3$, $La_{0.67}Ca_{0.33}Mn_{0-y}Al_yO_3$ and so on [48, 49].

On the analogy of these manganites, $Nd_{1-x}Pb_xMnO_3$ is also expected to contain this ferromagnetism at $T > T_c$. In fact, the increase in the amount of Mn^{3+} by Pb substitution raises T_c and increases χ. This is the evidence for short-range ferromagnetism in $Nd_{1-x}Pb_xMnO_3$ ($x \leqslant 0.25$) above T_c. In the paramagnetic regime at $T > T_p$, short-range ferromagnetism becomes weak and eventually disappears. In the intermediate region, then, the transfer integral enhanced by the DE interactions leads to the reduction of W_H, and W_H decreases with increasing x because the increase in the number of Mn^{3+} ions strengthens the DE interactions. Furthermore, this short-range ferromagnetism must be predominantly responsible for the deviation from the Curie–Weiss law at $T < T_p$ [5, 23]. An argument like this does not contradict the increase in the activation energy required for the electronic conduction in $LaMnO_3$ doped by nonmagnetic Ga which suppresses the DE mechanism [50].

In comparison with the paramagnetic regime at $T > T_p$, the trapping energy W_O is high and increases with x in the intermediate region. Since W_O is the potential difference between a polaron bound to a trap and a free polaron, either a fall of the potential level of the polaron bound to a trap or a rise of that of the free polaron leads to a high trapping energy. At the moment, however, it is still unknown which potential change is more predominant in the intermediate region, but the trapped state of the polaron seems difficult to change by the DE interactions.

4.3. Conduction change around T_c

As shown in figure 4, the bulk conduction changes at T_c in the specimens with $x = 0.10$ and 0.25. Other specimens ($x = 0.15$ and 0.20) exhibit the same behaviour. Furthermore, there is a very feeble inflexion around T_c at $x = 0.20$ in both the bulk conduction and the Arrhenius relation of $f_{\varepsilon''_{max}}$ and $1/T$ in figure 7, and it shows up rather clearly at $x = 0.25$ as shown in figures 4 and 7, so that this inflexion is found even in four-probe dc conductivity at $x = 0.25$. The argument in the previous section assures that the DE interactions work effectively in the present system at $T < T_p$. It appears difficult, however, to describe the conduction around T_c at $x \leqslant 0.25$ using only the DE interactions because every specimen exhibits insulating behaviours due to a hopping process of small polarons which are stabilized by the EP interactions or the JT effect. The DE mechanism is believed to be one of the important factors that dominate the MI transition in most manganites. As described in the introduction, $NdMnO_3$ is more strained than $LaMnO_3$. Though the partial substitution of Pb^{2+} for Nd^{3+} eases the lattice distortion, $Nd_{1-x}Pb_xMnO_3$ is still distorted when x is small. A long Mn–O bond length and rather large deviation of Mn–O–Mn bond angle from 180° due to such lattice distortion suppress the DE interactions. However, a reduction of the lattice distortion by increasing the amount of Pb activates the DE interactions. At $x \geqslant 0.20$, the DE interactions must be competitive with the EP interactions or the JT distortion around T_c, and then the DE interactions must play an important role in the conduction around T_c.

In less strained lattices, the DE mechanism correlating strongly with the MI transition is active. In fact, $La_{1-x}A_xMnO_3$ shows the typical MI transition even if x is very small whereas a marked emergence of the MI transition in $Nd_{1-x}A_xMnO_3$ requires a large value for x [9, 51]. This is because $Nd_{1-x}A_xMnO_3$ is more distorted than $La_{1-x}A_xMnO_3$ [32]. In strained lattices in which the DE interactions are suppressed, the EP interactions are active and the insulating conduction occurs. Consequently, the emergence of the inflexion around T_c in the bulk conduction of $Nd_{1-x}Pb_xMnO_3$ is very sensitive to the subtle competition between the DE and EP interactions.

The physics in many manganites has to take account of charge ordering at $T < T_c$. Because of anomalous magnetic behaviours below T_c observed in figure 1, one also expects charge ordering in $Nd_{1-x}Pb_xMnO_3$ even at $x \leqslant 0.25$. However, the discussion on the correlation between charge ordering and the conduction in this composition range at $T < T_c$ is postponed until the detailed knowledge of charge ordering at $x \leqslant 0.25$ is available. In fact, even the relation of $\varepsilon''_{max} \cdot T$ and $1/T$ is still unknown at $T < T_c$, as shown in figure 8.

5. Conclusion

Measurements of the bulk conductivity and the dielectric relaxation processes by the ac method including complex-plane impedance analysis and four-probe dc conductivity, along with the measurement of the magnetic susceptibility, have been carried out on insulating $Nd_{1-x}Pb_xMnO_3$ ($x = 0.10, 0.15, 0.20$ and 0.25). In the bulk conduction of each specimen, there are three temperature regimes where different processes dominate the electronic conduction:

(i) the paramagnetic regime above T_p,
(ii) the intermediate regime between T_p and the ferromagnetic ordering temperature T_c and
(iii) the temperature regime below T_c, where T_p is the temperature which marks the onset of deviation of χ^{-1} from the Curie–Weiss law.

The appreciable transition from the high-temperature regime to the intermediate one is found around T_p in the bulk conduction and the temperature dependence of the dielectric loss factor,

but never in dc measurements. Both of the bulk conductions in the high-temperature regime at $T > T_p$ and the intermediate-temperature regime between T_p and T_c are described by a hopping process of adiabatic small polarons. The dielectric relaxation process obtained in ac measurements also assures the polaronic scenario in these temperature regimes.

In comparison with the high-temperature regime, however, the hopping energy W_H is low and decreases more rapidly with x increasing in the intermediate regime. The low hopping energy at $T < T_p$ is ascribed to the double-exchange mechanism due to magnetic coupling between Mn^{3+} and Mn^{4+} through O^{2-} because the double-exchange interactions result in short-range ferromagnetism and then increase the electron transfer integral. An inflexion shows up around T_c in the bulk conduction at $x \geqslant 0.2$. This anomaly around T_c must be due to the subtle competition between the double-exchange and electron–phonon interactions. The double-exchange interactions are susceptibly dependent on the lattice parameters such as Mn–O bond length and Mn–O–Mn bond angle. This speculation has been evidenced with the ac results obtained by changing x in $Nd_{1-x}Pb_xMnO_3$.

Acknowledgments

The authors are very grateful to H Satoh and Y Morishita for their assistance in this project. This project was supported by a Grant-in Aid for Science Research (No. 11650716) from the Ministry of Education, Science and Culture, Japan, and also by Seimi Chemical Co., Ltd.

References

[1] Jonker G H and Santen J H V 1950 *Physica* **16** 337
[2] Chahara K, Ohno T, Kasai M, Kanoe Y and Kozono Y 1993 *Appl. Phys. Lett.* **62** 780
[3] Jin S, Tiefel T H, McCormack M, Fastnacht R A, Ramesh R and Chen L H 1994 *Science* **264** 413
[4] Tomioka Y, Asamitsu A, Moritomo Y, Kuwahara H and Tokura Y 1995 *Phys. Rev. Lett.* **74** 5108
[5] De Teresa J M, Ibarra M R, Algarabel P A, Ritter C, Marquina C, Blasco J, Garcia J, del Moral A and Arnold J 1997 *Nature* **376** 256
[6] Torrance J B, Lacorre P and Nazzal A I 1992 *Phys. Rev.* B **45** 8209
[7] Hwang H Y, Cheong S-W, Radaeli P G, Marezio M and Batlogg B 1995 *Phys. Rev. Lett.* **75** 914
[8] Zener C 1951 *Phys. Rev.* **82** 403
[9] Kusters R M, Singleton J, Keen D A, McGreevy R and Hayes W 1989 *Physica* B **155** 362
[10] Von Helmolt R, Wecker J, Holzapfel B, Schultz L and Samwer K 1993 *Phys. Rev. Lett.* **71** 2331
[11] Mandal P, Bärner K, Haupt L, Poddar A, Von Helmolt R, Jansen A G M and Wyder P 1998 *Phys. Rev.* B **57** 10256
[12] Mills A J, Littlewood P B and Sharinman B I 1995 *Phys. Rev. Lett.* **74** 5144
[13] Mills A J, Sharinman B I and Mueller R 1996 *Phys. Rev. Lett.* **77** 175
[14] Goodenough J B 1997 *J. Appl. Phys.* **81** 5330
[15] Chen C H, Cheong S-W and Cooper A S 1993 *Phys. Rev. Lett.* **71** 2461
[16] Tomioka Y, Asamitsu A, Moritomo Y and Tokura Y 1995 *J. Phys. Soc. Japan* **64** 5144
[17] Urushibara U, Moritomo Y, Arima T, Asamitsu A, Kido G and Tokura Y 1995 *Phys. Rev.* B **51** 14103
[18] Vogt T, Cheetham A K, Mahendiran R, Raychaudhuri A K, Mahesh R and Rao C N R 1996 *Phys. Rev.* B **54** 15303
[19] Radaelli P G, Cox D E, Marezio M and Cheong S-W 1997 *Phys. Rev.* B **55** 3015
[20] Nojiri H, Kaneko K, Motokawa M, Hirota K, Endoh Y and Takahashi K 1999 *Phys. Rev.* B **60** 4142
[21] De Teresa J M, Ibarra M R, Blasco J, Garcia J, Marquina C and Algarabel P A 1996 *Phys. Rev.* B **54** 1187
[22] Ibarra M R, Algarabel P A, Marquina C, Blasco J and Garcia J 1995 *Phys. Rev. Lett.* **75** 3541
[23] Shimomura S, Tajima K, Wakabayashi N, Kobayashi S, Kuwahara H and Tokura Y 1998 *J. Phys. Soc. Japan* **68** 1943
[24] Bauerle J E 1969 *J. Phys. Chem. Solids* **30** 2657
[25] MacDonald J R 1974 *J. Chem. Phys.* **61** 3977
[26] MacDonald J R 1976 *Superionic Conductors* (New York: Plenum) p 1
[27] Franklin A D 1975 *J. Am. Ceram. Soc.* **58** 465

[28] Iguchi E, Ueda K and Jung W H 1996 *Phys. Rev.* B **54** 17431
[29] Iguchi E, Nakamura N and Aoki A 1998 *Phil. Mag.* **78** 65
[30] Iguchi E, Tokuda Y, Nakatsugawa H and Munakata F 2002 *J. Appl. Phys.* **91** 2149
[31] Iguchi E 2002 Electronic transport properties in transition metal oxides *Recent Research Developments in Physics and Chemistry of Solids* ed S G Pandalai (Trivandrum: Transworld Research Network) p 159
[32] Liu K, Wu X W, Ahn K H, Sulchek T, Chien C and Xiao J Q 1996 *Phys. Rev.* B **54** 3007
[33] Iguchi E, Nakatsugawa H and Futakuchi K 1998 *J. Solid State Chem.* **58** 755
[34] Iguchi E, Nakatsugawa H, Satoh H and Munakata F 1999 *Physica* B **270** 332
[35] Nakatsugawa H and Iguchi E 1999 *J. Phys.: Condens. Matter* **11** 1711
[36] Thomas R-M, Skumryev V, Coey J M D and Wirth S 1999 *J. Appl. Phys.* **85** 5384
[37] Lalevic B, Fuschillo N and Wang W 1974 *Appl. Phys.* **5** 127
[38] Iguchi E, Kubota N, Nakamori T, Yamamoto N and Lee K J 1991 *Phys. Rev.* B **43** 8646
[39] Iguchi E and Akashi K 1992 *J. Phys. Soc. Japan* **61** 3385
[40] Lee K J, Iguchi A and Iguchi E 1993 *J. Phys. Chem. Solids* **54** 975
[41] Iguchi E and Jung W H 1994 *J. Phys. Soc. Japan* **63** 3078
[42] Hennion M, Moussa F, Rodriguez-Carvajal J, Pinsard L and Revcolevschi A 1997 *Phys. Rev.* B **56** R497
[43] Allodi G, De Renzi R and Guidi G 1998 *Phys. Rev.* B **57** 1024
[44] Lang I G and Firsov Yu A 1968 *Zh. Eksp. Teor. Fiz.* **54** 826
[45] Austin I G and Mott N F 1969 *Adv. Phys.* **18** 41
[46] Emin D and Holstein T 1969 *Ann. Phys.* **53** 439
[47] Fröhlich H 1958 *Theory of Dielectric* (Oxford: Clarendon) p 70
[48] Cai J-W, Wang C, Shen B-G, Zha J-G and Zhan W-S 1997 *Appl. Phys. Lett.* **71** 1727
[49] Blasco J, Garcia J, De Teresa J M, Ibarra M R, Perez J, Algarbel P A, Marquina C and Ritter C 1997 *Phys. Rev.* B **55** 8905
[50] Sun Y, Xu X, Zheng L and Zhang Y 1999 *Phys. Rev.* B **60** 12317
[51] Clausen K N, Hayes W, Keen D A, Kusters R M, McGreevy R L and Singleton J 1989 *J. Phys.: Condens. Matter* **1** 2721